Hindawi Publishing Corporation
Journal of Spectroscopy
Volume 2015, Article ID 618279, 7 pages
http://dx.doi.org/10.1155/2015/618279

Research Article

Oxide Nanolayers in Stratified Samples Studied by X-Ray Resonant Raman Scattering at Grazing Incidence

Juan José Leani,[1] Héctor Jorge Sánchez,[1,2] and Carlos Alberto Pérez[3]

[1] *Facultad de Matemática Astronomía y Física, Universidad Nacional de Córdoba, 5000 Córdoba, Argentina*
[2] *CONICET, Argentina*
[3] *Laboratorio Nacional de Luz Síncrotron, CP 6192, 13084-971 Campinas, Brazil*

Correspondence should be addressed to Juan José Leani; newjuanjo@gmail.com

Received 23 October 2014; Accepted 16 February 2015

Academic Editor: Rafal Sitko

Copyright © 2015 Juan José Leani et al. This is an open access article distributed under the Creative Commons Attribution License, which permits unrestricted use, distribution, and reproduction in any medium, provided the original work is properly cited.

X-ray resonant Raman scattering is applied at grazing incidence conditions with the aim of discriminating and identifying chemical environment of iron in different layers of stratified materials using a low resolution energy dispersive system. The methodology allows for depth studies with nanometric resolution. Nanostratified samples of Fe oxides were studied at the Brazilian synchrotron facility (LNLS) using monochromatic radiation and an EDS setup. The measurements were carried out in grazing incident regime with incident photon energy lower than and close to the Fe-K absorption edge. The result allowed for characterizing oxide nanolayers, not observable with conventional geometries, identifying the oxidation state present in a particular depth of a sample surface with nanometric, or even subnanometric, resolution using a low-resolution system.

1. Introduction

X-rays are totally reflected if the incident radiation angle is less than the critical angle, as the refractive index is less than unity [1]. Even when X-rays are theoretically reflected, an evanescent wave penetrates the first atomic layers of the surface [2]. Different depths of a sample surface can be analyzed using this fact, by means of scanning the incident X-ray beam angle in the vicinity of the critical angle. Consequently, a proper analysis of characteristic emissions or reflected intensity offers a tool for studying several properties of the sample surface, such as variations of electron densities, reaching special resolutions from Ångströms to hundred-nanometer deep [3]. Using this total reflection geometry, a number of papers have been published showing the potentiality of this effect combined with other techniques in a variety of samples and energy ranges [1, 4–11].

Different kinds of processes take place when atoms interact with X-rays and even some second-order interactions can become important under particular experimental situations, as resonant conditions. An example of such process is the X-ray resonant Raman scattering (RRS) [12].

With the aim of understanding better the physical processes involved in this atomic interaction, an early depiction of the resonant Raman scattering is found in the following time-depending perturbation theory expression [13]:

$$H_{\text{int}} = \sum_j \frac{e^2}{2mc^2} \cdot A_j^2 - \sum_j \frac{e}{mc} \cdot \left(p_j \cdot A_j\right), \tag{1}$$

where p_j is the momentum of the jth electron in the target sample and A_j is the vector potential of the electromagnetic field. The A^2 term allows for scattering process (including diffraction and nonresonant inelastic scattering), while the $p \cdot A$ term is responsible for absorption and resonant scattering processes.

The RRS interaction can be depicted using a 3-step process (Figure 1): an incident photon (of energy E_0) excites an inner shell electron (in this work 1s electron) to an unoccupied state above the Fermi level. The virtual intermediate state involves a 1s core hole and an excited photoelectron. In this "virtual transition" the energy of the incident photon can be smaller than the binding energy of the excited electron. The

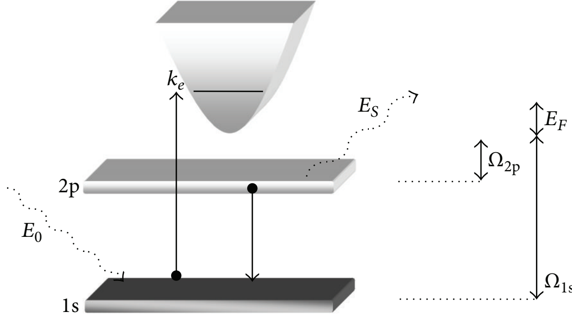

Figure 1: Schematic representation of a 2p → 1s X-ray resonant Raman scattering process.

final state is reached filling up the 1s core hole with and outer-shell electron (in this work 2p electron) and emitting a photon (of energy E_S), leaving subsequently a hole in the 2p subshell and a photoelectron above the Fermi level. In this way, the energy conservation for the whole process demands the following [15]:

$$E_0 = \Omega_L + E_f + E_S + k_e, \quad (2)$$

where Ω_L is the binding energy of 1s electrons, E_f is the Fermi energy, E_S is the energy of the emitted photon, and k_e is the kinetic energy of the photoelectron. The last equation reveals an interesting feature of the RRS process: since the photoelectron and the emitted photon have to share the available energy, when this atomic process occurs, a variety of emitted photon energies are possible for a single-incident-photon energy.

Inelastic X-ray scattering is nowadays a useful process that allowed the creation of several powerful techniques for researching electronic properties of atomic and molecular systems. A more detailed structural discrimination is one of the main advantages that this inelastic X-ray spectroscopy presents, since eliminating the natural width due to the finite live-time of the 1s hole is possible working in resonant conditions. More specifically, this novel RRS technique allows for reaching local atomic information, as in XANES spectroscopy, employing monochromatic exciting radiation in combination with high-resolution systems [16–21]. In addition, the combination of RRS and grazing incidence excitation allows for performing surface analysis and depth profiling [22].

Nanostratified samples of different Fe compounds were studied at the Brazilian synchrotron facility. The measurements were carried out in total reflection geometry scanning the incident radiation angle around the critical angle with incident energy lower than and close to the K absorption edge of Fe in order to study the RRS emissions of each layer.

The RRS spectra were analyzed with programs for fitting the experimental data to a theoretical expression. After that, the determined residuals were treated with a FFT smoothing process, with the aim of taking into account the instrument function of the detecting system. Finally, these RRS residuals show oscillation patterns that change as a function of the observed depth, allowing for spatially discriminated studies of the chemical environments in nanolayers with nanometric, and even subnanometric, resolution.

The results presented in this work demonstrate that X-ray resonant Raman scattering in total reflection geometry represents a new and useful spectrometric tool. It allows to obtain detail structural information in stratified materials using a low-resolution EDS system.

2. Measurements and Data Processing

The measurements were carried out at XRF station of the D09BXRF beamline [23] at the Brazilian synchrotron facility (LNLS, Campinas) [24].

The detector used was a KETEK AXAS-A solid-state detector (energy resolution of 139 eV for the Mn-Kα line). Pulse processing was accomplished by a fast amplifier with triangular shaping and spectra were processed and collected with an 8 K MCA. The flux on sample was 10^8 ph s^{-1} @ 10 keV (monitored with ionization chambers). The exciting radiation was collimated to 1 × 1 mm using slits. XRF beamline was equipped with a double crystal "channel-cut" monochromator (energy resolution ≈ 3 eV at 10 keV) using a Si(111) crystal.

The samples consisted of two pure Fe foils (>0.999) with a thickness of 0.1 mm. On top of them, different layers were deposited by sputtering the following.

Sample A. A 10 nm Fe layer (heated after sputtering at 200°C during 1 hour) and a 200 nm Fe layer (deposited and maintained at room temperature, ~20°C) both were deposited in an O_2 atmosphere (20%).

Sample B. A 5 nm Fe layer, in O_2 atmosphere (20%), and a 50 nm Fe layer, in O_2 atmosphere (5%), both were deposited at room temperature (~20°C).

The samples were irradiated with monochromatic photons of 7072 eV, that is, 40 eV below the K absorption edge of Fe with the aim of properly exciting the Raman process. Although when an exciting energy far away from the absorption edge significantly decreases the RRS cross section (i.e., its intensity) [25], an incident photon energy very close to the K-threshold energy causes that the shape of the X-ray Raman peak approaches to the thinner fluorescence peak [26], where the RRS oscillations could be observed only utilizing very-high-resolution systems.

A scanning of the incident radiation angle around the critical angle was performed in both samples.

The depth, measured perpendicularly from the sample surface, at which the intensity of the incident radiation is reduced to $1/e$ of its initial value, is [3]

$$z_{1/e} = \frac{\lambda}{4\pi B}, \quad (3)$$

where λ is the wavelength of the incident photon and B is

$$B = \frac{1}{\sqrt{2}} \left\{ \left[\left(\varphi^2 - \varphi_c^2\right)^2 + 4\beta^2 \right]^{1/2} - \left(\varphi^2 - \varphi_c^2\right)^{1/2} \right\} \quad (4)$$

with φ being the incident beam angle, φ_c the critic angle for the analyzed media, $\beta = \mu\lambda/4\pi$ is the imaginary part of the refractive index, and μ is the linear absorption coefficient.

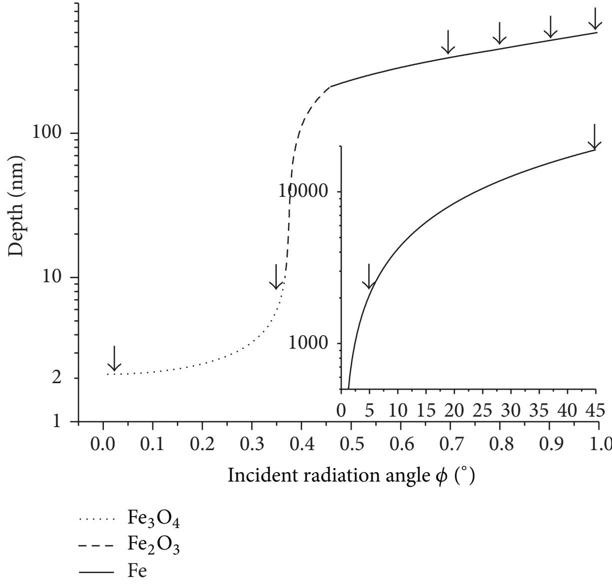

FIGURE 2: Calculated penetration depth (3) as a function of the incident radiation angle for sample A. Incident radiation energy 7072 eV. Irradiation angles are also plotted.

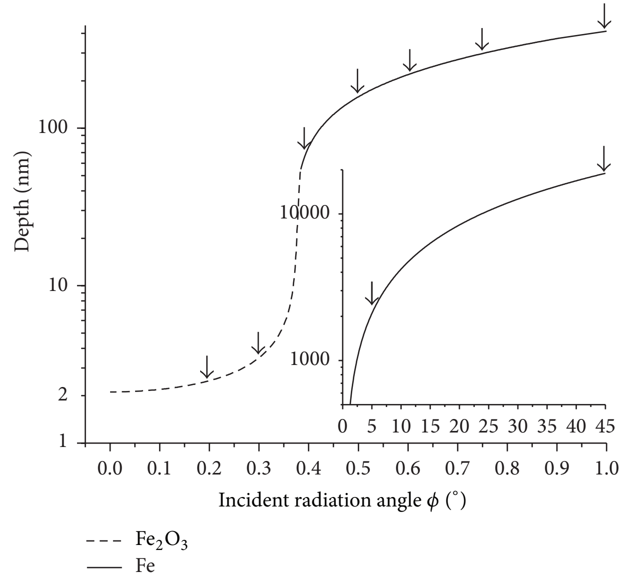

FIGURE 3: Calculated penetration depth (3) as a function of the incident radiation angle for sample B. Incident radiation energy 7072 eV. Irradiation angles are also plotted.

The critic angle φ_c is given by [1]

$$\varphi_c = \sqrt{2\delta} \tag{5}$$

which is derived from Snell's law. δ, the real part of the refractive index, could be represented as

$$\delta = \frac{ne^2\lambda^2}{2\pi mc^2}, \tag{6}$$

where n is the total number of dispersive electrons per unit volume:

$$n = N\left(\frac{Z}{A}\right)\rho, \tag{7}$$

where N is the Avogadro's number, Z is the atomic number, A is the atomic weight, and ρ is the sample density.

Figures 2 and 3 show the calculated penetration depth (Equation (3)) as a function of the incident beam angle for the surface layer of samples A and B, respectively (incident photon energy of 7072 eV). The irradiation angles are also indicated.

As could be appreciated, the observed depth just increases a few Ångströms when the incident angle goes from 0° to ~0.25°. This feature, due to that fact that the reflected intensity changes very smoothly with the incident radiation angle far away from the critical angle, can be used for performing a detailed analysis of the most external layers of the sample.

The rust present in a metal has a volume higher than the volume of the originating mass of sample, since oxidation results in an attenuated electron density.

In this respect, the calculated observed depths are estimations. The electron density reduction in respect of a nonoxidized surface induces a discrepancy in the calculated δ value, with this discrepancy being carried to the $z_{1/e}$ value. Moreover, loose packing, porosity, and other effects could cause the penetration to be somewhat greater than the calculated value, with these effects being very difficult to take into account and to quantify. In any case, the considerations made before do not represent a problem for our analysis. The purpose of this paper is to show the potentiality of RRS spectroscopy in grazing incident conditions as a new tool in order to study changes of chemical environments with depth, with the calculated values being good enough for our survey.

The incident radiation angles and the corresponding calculated depths were as follows:

sample A: 0,01° (~2,12 nm); 0,35° (~6,05 nm); 0,7° (~332 nm); 0,8° (~379 nm); 0,9° (~4,11 nm); 1° (~500 nm); 5° (~2114 nm); 45° (~19141 nm),

sample B: 0,2° (~2,45 nm); 0,3° (~3,5 nm); 0,4° (~68 nm); 0,5° (~152 nm); 0,6° (~220 nm); 0,75° (~295 nm); 1° (~411 nm); 5° (~2100 nm); 45° (~18958 nm).

The measuring livetime for each point was 600s. Irradiation angles are also indicated in Figures 2 and 3.

Values of μ are extracted from Hubbell and Seltzer [27] and values of ρ are taken from Lide [28].

Spectra were analyzed with specific programs [29, 30]. The data fitting of the low-energy side of Raman peaks was achieved using a Lorentzian expression:

$$y = y_0 + \frac{2A}{\pi}\frac{\omega}{4\left(x - x_0\right)^2 + \omega^2}, \tag{8}$$

where y_0 is the baseline offset, A is the area under the curve (from the baseline), x_0 is the center of the peak, and ω is the full width at half height (FWHM) of the peak. A comparison

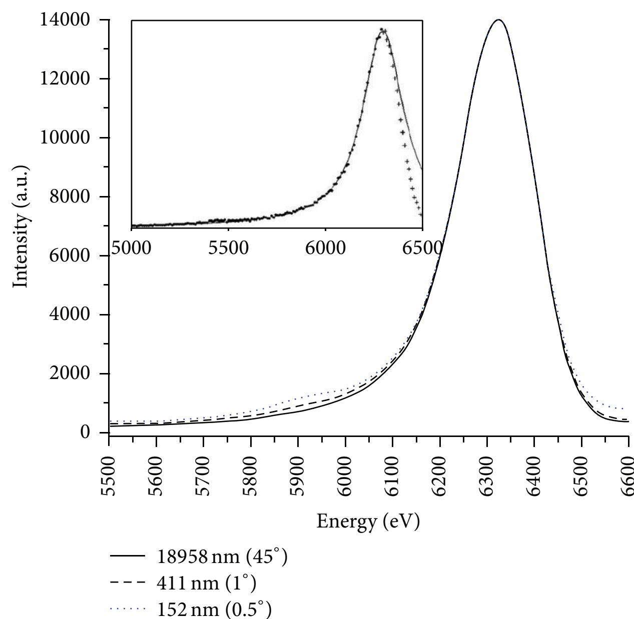

Figure 4: Comparison between Raman spectra obtained at three different observed depths in sample B. Inset: example of Lorentzian fit in the Raman tail.

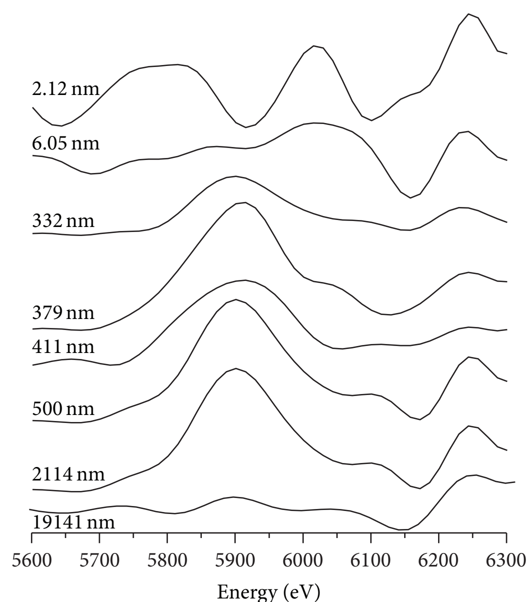

Figure 5: Residuals between experimental Raman spectra and the data fitting as a function of the studied depth for sample A.

between Raman spectra obtained at three different observed depths (152 nm, 411 nm, and 18958 nm) is shown in Figure 4 for sample B. An example of Raman tail fit using a Lorentzian decay is also shown inset.

In this work, a standard denoising method was employed based on the frequency decomposition of the signal [31]. An FFT smoothing procedure was applied considering a Gaussian instrumental function with an σ of 59 eV. This smoothing procedure is accomplished by removing Fourier components with frequencies larger than $(1/n\Delta t)$, where n is the number of data points considered at a time and Δt is the time spacing between two adjacent data points. It works as a perfect low-pass filter where the cutoff frequency plays the role of a parameter during the analysis since, by suppressing the high-frequency components, the noise associated with them can be eliminated. A detailed description of the analysis of resonant Raman spectra and the Raman residuals can be found in [32].

3. Results and Discussion

As it was expected, at this incident energy, the Raman peak is intense dominating over the Compton peak, since the Raman cross section is resonantly enhanced [33].

The results presented in this paper do not take into account bremsstrahlung or infrared divergence contributions, since their contributions are significant mainly in low energy regions and do not affect appreciably the range of the RRS emissions here studied [34]. Furthermore, these processes have the same energy distribution in the analyzed layers, being compensated in comparison with the RRS residuals.

In this work it is assumed that the absorption phenomenon is comparatively weak since both incident and emitted energies are below the K-threshold, exempting the need of self-absorption corrections [35].

Low absorption allows for reaching a bigger penetration in sample, allowing for improved depth studies. Besides, low deposited doses are extremely valuable to study X-ray susceptible samples, as biological ones.

Figures 5 and 6 show the low-energy residuals between the experimental Raman spectra and the theoretical fitting, (8), as a function of the observed depth for samples A and B, respectively.

Figure 7 presents the residuals between experimental Raman spectra and data fitting for pure Fe compounds. These pure compounds were measured from compacted powder in conventional geometry (45°-45°) [14].

A notable resemblance can be appreciated between the oscillation patterns present in the residuals of the measured oxidized layers in both samples (Figures 5 and 6) and reference patterns (Figure 7). From a simple and qualitative inspection, relevant information could be obtained.

The oscillation pattern belongs to the most external layer of sample A (Figure 5) present in mark oscillation peaks at ~6000 eV and ~5770 eV, corresponding to the pattern of Fe_3O_4 in the reference data (Figure 7). Otherwise, the layer immediately below presents a single oscillation peak at ~ 5900 eV, corresponding to the pattern of Fe_2O_3 (Fe(III)) in the reference patterns. The deeper layer (bulk) reveals a smooth pattern, lacking prominent oscillations, similar to the one corresponding to pure Fe in reference data of Figure 7. The result says that the most superficial layer, deposited at 200°C, seems to be oxidized as Fe_3O_4 (Fe(II,III)), while the intermediate layer, deposited at room temperature in the same O_2 atmosphere, seems to be oxidized as Fe_2O_3 (Fe(III)).

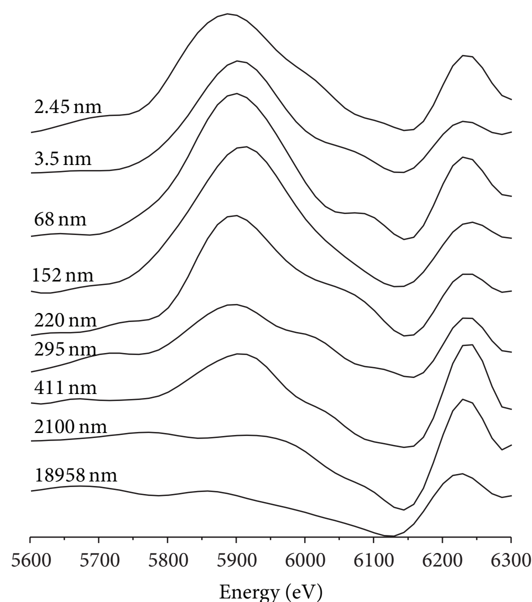

Figure 6: Residuals between experimental Raman spectra and the data fitting as a function of the studied depth for sample B.

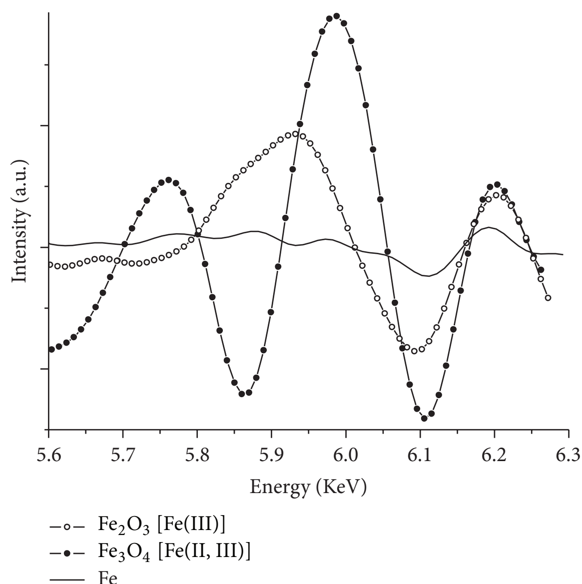

Figure 7: Residuals between experimental Raman spectra and data fitting for pure Fe compounds measured from compacted powder in conventional geometry (45°-45°) [14].

These results have a consistent behavior with previous work [36].

In the case of sample B (Figure 6), both the most external and intermediate layers present a single mark oscillation peak at ~5900 eV, similar to the one corresponding to Fe_2O_3 in reference patterns (Figure 7). The oscillation pattern corresponding to the Fe foil reveals a smooth oscillation pattern as pure Fe in reference measurements. The result shows that both the superficial, deposited in O_2 atmosphere (20%), and intermediate, deposited in O_2 atmosphere (5%), layers seem to be oxidized as Fe_2O_3(Fe(III)), both deposited at the same room temperature. These results say that the oxygen availability at the moment of the oxidation process can accelerate the rate of oxide formation but does not change the oxidation state if the deposition is realized at the same temperature.

In both foils, the substrate signal indicates that the Fe substrate seems to conserve its pure state.

As mentioned in the previous section, the calculated depths showed in Figures 2 and 3 are approximations and correlate with the experimental results approximately. In particular, some layers seem to be thicker than theory predictions. In addition to the facts mentioned before during the fabrication process, deeper layers are exposed to heat and oxidation atmospheres during the sputtering procedure, resulting probably in additional oxidation process that is not taken into account. On the other hand, a somehow undefined interface layer prevents strong interference effects due to standing waves appearance.

Nevertheless, it is remarked again that the aim of this work is to show the potentiality of RRS spectroscopy in grazing incidence conditions as a new tool in order to study changes of chemical states with depth. In this context the theoretical model is precise enough for our study.

Thus this novel RRS tool in grazing incidence geometry not only allowed for observing and separating between thin oxide Fe layers (not observables with conventional geometries) but it also allowed for the identification of the oxide states present in these layers.

Furthermore, in stratified sample studies, due to the fact that the reflected intensity changes smoothly with the incident radiation angle close to the surface, a fine depth profiling provides a tool to determine the position and width of the oxidation state of each layer, or any layer with different chemical environment of the absorbing atom, with nanometric, or even subnanometric, resolution.

As a final point, experiences performed using low-resolution EDS systems, as that used in this work, require shorter measuring times than the typical ones utilizing high resolution systems (WDS spectrometers). Furthermore, the typical back-diffraction geometry (used to reach high resolution in WDS systems) does not allow the acquisition of the entire Raman spectrum from several elements, with this kind of surveys being unfeasible in those cases.

4. Conclusions

In this work, different iron oxides were speciated in nanolayers of stratified materials by using resonant Raman scattering in combination with grazing incidence techniques. The oscillation patterns of RRS spectra obtained from surface nanolayers of Fe(II) and Fe(III) were used to discriminate the species successfully. Considering similar samples and sample preparations, these results are in agreement with previous results reported by other authors.

This work shows an application of RRS spectroscopy at grazing incident condition as a tool to reach characterizations of chemical environments in nanostratified samples of iron using a low-resolution EDS setup. Several techniques are

combined in order to obtain specific results that could not be obtained using those techniques individually.

Since RRS spectroscopy is an emission technique, several studies are possible from the combination of X-ray resonant Raman scattering with other X-ray techniques and/or irradiation geometries. For instance, if the surface layers are parallel planes to the surface (e.g., stratified media), this technique could provide a precise determination of the width and position of the different oxide layers or layers with different chemical environment.

To the application of this tool for characterization of chemical environments in multiple experimental conditions (as in 3D confocal arrangements) and the turning of this novel tool into a complete analytical technique is pointed out our current research.

Finally, the flexible RRS technique will offer the remarkable chance of investigating electron density changes in a variety of materials and general samples at the nanomicroregime, reaching a characterization unfeasible to accomplish by current procedures.

Conflict of Interests

The authors declare that there is no conflict of interests regarding the publication of this paper.

Acknowledgment

This work was partially supported by the Laboratorio Nacional de Luz Sincrotron (Campinas, Brazil).

References

[1] E.-E. Koch, Ed., *Handbook on Synchrotron Radiation 1A*, North-Holland, Amsterdam, The Netherlands, 1983.

[2] M. Born and E. Wolf, *Principles of Optics*, Pergamon Press, New York, NY, USA, 1980.

[3] L. G. Parrat, "Surface studies of solids by total reflection of X-rays," *Physical Review*, vol. 95, p. 359, 1954.

[4] M. Tolan, *X-Ray Scattering from Soft-Matter Thin Films*, Springer, Berlin, Germany, 1999.

[5] A. Iida, A. Yoshinaga, K. Sakurai, and Y. Gohshi, "Synchrotron radiation excited X-ray fluorescence analysis using total reflection of X-rays," *Analytical Chemistry*, vol. 58, no. 2, pp. 394–397, 1986.

[6] C. Vázquez, S. Boeykens, and D. Elkin, "The use of total reflection X-ray fluorescence in an underwater archaeology case study," *Technical Briefs in Historical Archaeology*, vol. 5, pp. 10–15, 2010.

[7] A. Prange, "Total reflection X-ray spectrometry: method and applications," *Spectrochimica Acta Part B: Atomic Spectroscopy*, vol. 44, no. 5, pp. 437–452, 1989.

[8] R. Klockenkämper and A. von Bohlen, "Total reflection X-ray fluorescence—an efficient method for micro-, trace and surface layer analysis. Invited lecture," *Journal of Analytical Atomic Spectrometry*, vol. 7, no. 2, pp. 273–279, 1992.

[9] R. Barchewitz, M. Cremonese-Visicato, and G. Onori, "X-ray photoabsorption of solids by specular reflection," *Journal of Physics C: Solid State Physics*, vol. 11, no. 21, article 019, pp. 4439–4445, 1978.

[10] B. M. Murphy, M. Müller, J. Stettner et al., "Investigating surface dynamics with inelastic X-ray scattering," *Journal of Physics Condensed Matter*, vol. 20, no. 22, Article ID 224001, 2008.

[11] T. T. Fister, D. D. Fong, J. A. Eastman et al., "Total-reflection inelastic x-ray scattering from a 10-nm thick $La_{0.6}Sr_{0.4}CoO_3$ thin film," *Physical Review Letters*, vol. 106, no. 3, Article ID 037401, 2011.

[12] A. G. Karydas and T. Paradellis, "Measurement of KL and LM resonant Raman scattering cross sections with a proton-induced X-ray beam," *Journal of Physics B: Atomic, Molecular and Optical Physics*, vol. 30, no. 8, pp. 1893–1905, 1997.

[13] G. Brown and D. E. Moncton, *Handbook on Synchrotron Radiation*, vol. 3, North Holland Publishing Company, 1991.

[14] J. J. Leani, H. Sánchez, M. Valentinuzzi, and C. Pérez, "Chemical environment determination of iron oxides using RRS spectroscopy," *X-Ray Spectrometry*, vol. 40, no. 4, pp. 254–256, 2011.

[15] J.-E. Rubensson, "RIXS dynamics for beginners," *Journal of Electron Spectroscopy and Related Phenomena*, vol. 110-111, pp. 135–151, 2000.

[16] J. Szlachetko, J.-Cl. Dousse, M. Berset, K. Fennane, and M. Szlachetko, "High-resolution study of the x-ray resonant Raman scattering process around the 1*s* absorption edge for aluminium, silicon, and their oxides," *Physical Review A*, vol. 75, no. 2, Article ID 022512, 11 pages, 2007.

[17] H. Hayashi, "Lifetime-broadening-suppressed selective XAFS spectroscopy," *Analytical Sciences*, vol. 24, no. 1, pp. 15–23, 2008.

[18] G. Dräger and P. Machek, "Numerical method for inverting 1_s2_p resonant inelastic x-ray scattering spectra: interpretation of hidden electronic excitations in CuO," *Physical Review B*, vol. 79, no. 3, Article ID 033103, 4 pages, 2009.

[19] H. Hayashi, "SIM-RIXS: a program to simulate resonant inelastic X-ray scattering," *X-Ray Spectrometry*, vol. 40, no. 1, pp. 24–30, 2011.

[20] M. Kavčič, M. Žitnik, K. Bučar, and J. Szlachetko, "Application of wavelength dispersive X-ray spectroscopy to improve detection limits in X-ray analysis," *X-Ray Spectrometry*, vol. 40, no. 1, pp. 2–6, 2011.

[21] F. Meirer, C. Streli, G. Pepponi et al., "Feasibility study of SR-TXRF-XANES analysis for iron contaminations on a silicon wafer surface," *Surface and Interface Analysis*, vol. 40, no. 12, pp. 1571–1576, 2008.

[22] J. J. Leani, H. J. Sánchez, R. D. Pérez, and C. Pérez, "Depth profiling nano-analysis of chemical environments using resonant Raman spectroscopy at grazing incidence conditions," *Analytical Chemistry*, vol. 85, no. 15, pp. 7069–7075, 2013.

[23] C. A. Pérez, M. Radtke, H. J. Sánchez et al., "Synchrotron radiation x-ray fluorescence at the LNLS: beamline instrumentation and experiments," *X-Ray Spectrometry*, vol. 28, no. 5, pp. 320–326, 1999.

[24] A. R. D. Rodrigues, R. H. A. Farias, M. J. Ferreira et al., "Commissioning and operation of the Brazilian synchrotron light source," in *Proceedings of the 17th Particle Accelerator Conference (PAC '97)*, pp. 811–813, Vancouver, Canada, May 1997.

[25] A. Kotani and S. Shin, "Resonant inelastic X-ray scattering spectra for electrons in solids," *Reviews of Modern Physics*, vol. 73, pp. 203–246, 2001.

[26] P. Eisenberger, P. M. Platzman, and H. Winick, "X-ray resonant Raman scattering: observation of characteristic radiation narrower than the lifetime width," *Physical Review Letters*, vol. 36, no. 11, pp. 623–626, 1976.

[27] J. M. Hubbell and S. M. Seltzer, *Tables of X-Ray Mass Absorption Coefficients and Mass Energy*, 5632, NISTIR, 1995.

[28] D. R. Lide, Ed., *Handbook of Chemistry and Physics*, CRC Press, Boca Raton, Fla, USA, 80th edition, 1999.

[29] SeaSolve Software, *PeakFit v4.12 for Windows*, SeaSolve Software, 2003, Portions Copyright 2000–2003 SYSTAT Software.

[30] TableCurve v1.11 for Windows, AISN Software, 1993.

[31] Q. Zhang, R. Aliaga-Rossel, and P. Choi, “Denoising of gamma-ray signals by interval-dependent thresholds of wavelet analysis,” *Measurement Science and Technology*, vol. 17, no. 4, pp. 731–735, 2006.

[32] J. J. Leani, H. J. Sánchez, M. Valentinuzzi, and C. Pérez, “Determination of the oxidation state by resonant-Raman scattering spectroscopy,” *Journal of Analytical Atomic Spectrometry*, vol. 26, no. 2, pp. 378–382, 2011.

[33] H. J. Sánchez, M. C. Valentinuzzi, and J. J. Leani, “Theoretical calculations of the influence of resonant Raman scattering on the quantification of XRF spectrochemical analysis,” *Journal of Analytical Atomic Spectrometry*, vol. 27, no. 2, pp. 232–238, 2012.

[34] Y. B. Bannett, D. C. Rapaport, and I. Freund, “Resonant x-ray Raman scattering and the infrared divergence of the compton effect,” *Physical Review A*, vol. 16, no. 5, article 2011, 1977.

[35] H. Hayashi, Y. Udagawa, W. A. Caliebe, and C.-C. Kao, “Lifetime-broadening removed X-ray absorption near edge structure by resonant inelastic X-ray scattering spectroscopy,” *Chemical Physics Letters*, vol. 371, no. 1-2, pp. 125–130, 2003.

[36] R. K. Gupta, K. Ghosh, R. Patel, and P. K. Kahol, “A novel method to synthesis magnetic thin film of iron oxide,” *Journal of Alloys and Compounds*, vol. 509, no. 27, pp. 7529–7531, 2011.

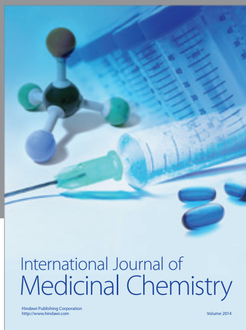
International Journal of
Medicinal Chemistry
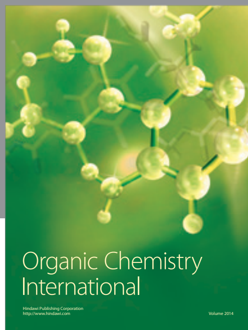
Organic Chemistry
International

International Journal of
Photoenergy

International Journal of
Analytical Chemistry
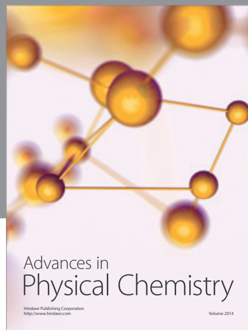
Advances in
Physical Chemistry
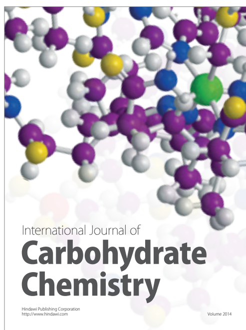
International Journal of
Carbohydrate Chemistry

Hindawi
Submit your manuscripts at
http://www.hindawi.com

Journal of
Quantum Chemistry

The Scientific
World Journal

Journal of
Analytical Methods
in Chemistry

Journal of
Spectroscopy

International Journal of
Inorganic Chemistry

International Journal of
Electrochemistry
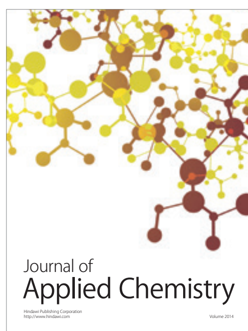
Journal of
Applied Chemistry
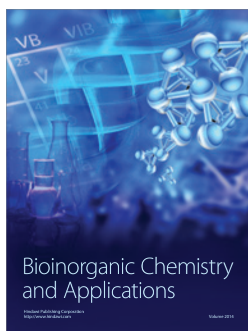
Bioinorganic Chemistry
and Applications
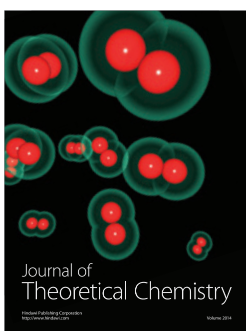
Journal of
Theoretical Chemistry
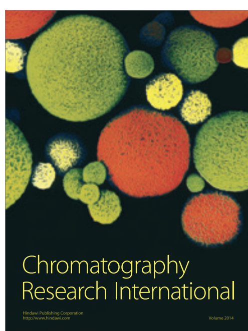
Chromatography
Research International

Journal of
Catalysts

Journal of
Chemistry

International Journal of
Spectroscopy